Second Order Generalized Integrator Based Reference Current Generation Method for Single-Phase Shunt Active Power Filters Under Adverse Grid Conditions

Saeed Golestan
Department of Electrical Engineering
Abadan Branch, Islamic Azad University
Abadan 63178-36531, Iran
Email: s.golestan@ieee.org

Mohammad Monfared
Department of Electrical Engineering
Ferdowsi University of Mashhad
Mashhad 91775-1111, Iran
Email: m.monfared@um.ac.ir

Josep M. Guerrero
Department of Energy Technology
Aalborg University
Aalborg DK-9220, Denmark
Email: joz@et.aau.dk

***Abstract*—The reference current generation (RCG) is a crucial part in the control of a shunt active power filter (APF). A variety of RCG techniques have been proposed in literature. Among these, the instantaneous reactive power theory, called pq theory, is probably the most widely used technique. The pq theory offers advantages such as satisfactory steady-state and dynamic performance, and at the same time simple digital implementation, however its application was limited to three-phase systems. To exploit the advantages of pq theory in single-phase systems, the single-phase pq theory has been proposed recently. In this paper, a simple and effective implementation of the single phase pq theory for single-phase shunt APFs is proposed. The suggested approach is based on employing second order generalized integrators (SOGI), and a phase locked loop (PLL). To fine tune the control parameters, a systematic design procedure based on the pole-zero cancellation, and the extended symmetrical optimum theory is proposed. During the design procedure, the effects of grid frequency variations and the presence of distortion in the grid voltage are taken into account. Finally, to confirm the effectiveness of the suggested approach, simulation results are presented.**

I. Introduction

Nowadays, with ever increasing use of power electronic-based devices/equipements, the harmonic contamination in electrical networks is growing rapidly. Harmonics increase the losses in electrical equipments, cause malfunction of protective devices, create interference with communication circuits, damage sensitive loads, and result in perturbing torque and vibration in electrical motors [1], [2]. Therefore, the compensation of harmonics has become a serious concern for both electricity suppliers and consumers [3].

To deal with harmonic problems, as well as to provide reactive power compensation, passive filters have been employed traditionally. These filters have a relatively low cost and high reliability, but they suffer from many disadvantages, such as large size, resonance susceptibility with the load and line impedances, de-tuning caused by aging, fixed compensating characteristics, etc [4]. Thus, in order to avoid these shortcomings, the active power filters (APFs) have attracted considerable attentions.

An APF is a power electronic converter-based device which is intended to mitigate the power quality problems caused by nonlinear loads. Several topologies for APFs have been proposed, with the most widely used being the shunt APFs (SAPFs) [5], [6]. As shown in Fig. 1, a SAPF is connected in parallel with the nonlinear load, and controlled to inject (draw) a compensating current, i_C, to (from) the grid such that, the source current, i_S, is an in-phase sinusoidal signal with the grid voltage, v_g, at the point of common coupling (PCC).

Extraction of the reference compensating current is undoubtedly the most crucial part in the control of a SAPF [7]. A variety of reference current generation (RCG) techniques has been proposed in literature. These approaches can be broadly classified into time-domain and frequency domain techniques.

The digital Fourier transform (DFT), fast Fourier transform (FFT), and sliding DFT (SDFT) (also known as recursive DFT (RDFT)) are the most renowned approaches in the frequency-domain [8]-[10]. These approaches provide a good precision in detecting harmonics, and can be applied to both single-phase and three-phase APFs. Despite these prominent advantages, the Fourier transform based approaches suffer from some common drawbacks such as: high computational burden, and high memory requirement [9]. Moreover, because of the relatively long time (typically more than two cycles of fundamental frequency) needed for computation of Fourier coefficients, these approaches are suitable for slowly varying load conditions [11].

The instantaneous active and reactive power theory (also called pq theory) is probably the most widely used time-domain RCG technique [12]. This theory was originally developed for three-phase, three-wire systems by Akagi et al. in 1983 [13], [14], and since then it has been significantly extended by different researchers [15], [16]. The pq theory has a relatively fast dynamic response and low computational burden compared to the frequency-domain approaches [9], but its application was limited to three-phase systems.

978-1-4673-4484-5/13/$31.00 ©2013 IEEE

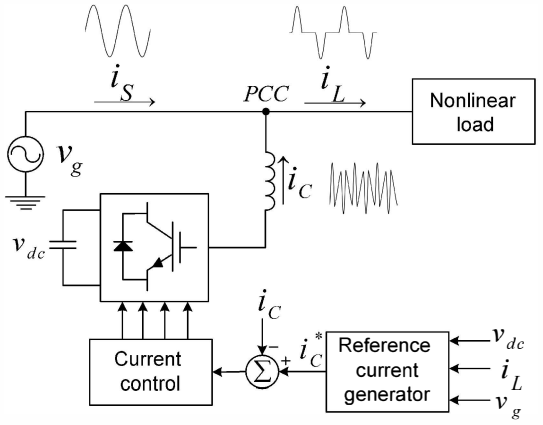

Fig. 1. A single-phase SAPF.

To exploit the advantages of the pq theory in single-phase APFs, the single-phase pq theory has been proposed in [17], [18]. In this theory, the load current and the grid voltage are shifted by $90°$, enabling the representation of the single-phase system as a pseudo two-phase ($\alpha\beta$) system. In this way, the three-phase pq theory can be applied to a single-phase system. A major drawback regarding this theory is that the grid voltage is considered as a pure sine wave. As a consequence, presence of any distortion in the grid voltage significantly degrades the extraction of the reference current. On the other hand, because of the frequency dependency of the techniques used to realize a phase shift of $90°$, variations of the grid frequency give rise to errors in the reference current estimation.

In this paper, a simple and effective implementation of the single phase pq theory for single-phase SAPFs is presented. The suggested approach is based on employing second order generalized integrators (SOGI), and a phase locked loop (PLL). To fine tune the control parameters, a systematic design procedure based on the pole-zero cancellation and the extended symmetrical optimum theory is proposed. During the design procedure, the effects of grid frequency variations and voltage distortions are taken into account. Finally, the effectiveness of the suggested approach is confirmed through simulation results.

II. Overview of Single-Phase pq Theory

In order to exploit the advantages of the pq theory in single-phase APFs, the single-phase pq theory has been proposed in [17], [18]. In this theory, the load current and the grid voltage at the point of common coupling (PCC) are shifted by $90°$, enabling the representation of the single-phase system as a pseudo two-phase ($\alpha\beta$) system. The original load current and grid voltage are considered as the α-axis quantities, whereas the $90°$ phase-shifted version of these signals are considered as the β-axis quantities. To achieve a phase shift of $90°$, different approaches such as using the all pass filter [18], the Hilbert transformation [20], and the transfer delay [21] have been proposed.

A common assumption in the single-phase pq theory is to consider the source voltage as a pure sine wave, i.e., $v_s(t) = V\cos(\omega t + \phi)$, where V, ω, and ϕ are the source voltage amplitude, frequency and phase angle, respectively. In this case, the $\alpha\beta$ coordinate representation of the source voltage is

$$\begin{bmatrix} v_{g\alpha}(\omega t) \\ v_{g\beta}(\omega t) \end{bmatrix} = \begin{bmatrix} v_g(\omega t) \\ v_g(\omega t - \pi/2) \end{bmatrix} = \begin{bmatrix} V\cos(\omega t + \phi) \\ V\sin(\omega t + \phi) \end{bmatrix}. \tag{1}$$

Similarly, the $\alpha\beta$ coordinate representation of the load current is

$$\begin{bmatrix} i_{L\alpha}(\omega t) \\ i_{L\beta}(\omega t) \end{bmatrix} = \begin{bmatrix} i_L(\omega t) \\ i_L(\omega t - \pi/2) \end{bmatrix}. \tag{2}$$

Once the β-axis quantities are obtained, the instantaneous active and reactive powers drawn by the nonlinear load can be expressed as

$$\begin{bmatrix} p \\ q \end{bmatrix} = \begin{bmatrix} \bar{p} + \tilde{p} \\ \bar{q} + \tilde{q} \end{bmatrix} = \begin{bmatrix} v_{g\alpha} & v_{g\beta} \\ -v_{g\beta} & v_{g\alpha} \end{bmatrix} \begin{bmatrix} i_{L\alpha} \\ i_{L\beta} \end{bmatrix} \tag{3}$$

where, p and q are the instantaneous active and reactive powers, respectively. The dc components $\bar{p}$ and $\bar{q}$ represent the fundamental active and reactive powers, respectively, and the ripple components $\tilde{p}$ and $\tilde{q}$ are the oscillating active and reactive powers, respectively.

The fundamental active current drawn by the nonlinear load can be obtained by taking the inverse of (3) as

$$\begin{bmatrix} {i'}_{L\alpha,p} \\ {i'}_{L\beta,p} \end{bmatrix} = \begin{bmatrix} v_{g\alpha} & v_{g\beta} \\ -v_{g\beta} & v_{g\alpha} \end{bmatrix}^{-1} \begin{bmatrix} \bar{p} \\ 0 \end{bmatrix} = \frac{1}{v_{g\alpha}^2 + v_{g\beta}^2} \begin{bmatrix} v_{g\alpha} \\ v_{g\beta} \end{bmatrix} \bar{p}. \tag{4}$$

Since, only the α-axis quantities are belong to the original single-phase system, therefore

$$i'_{L,p} = i'_{L\alpha,p} = \frac{\bar{p}}{v_{g\alpha}^2 + v_{g\beta}^2} v_{g\alpha}. \tag{5}$$

The reference compensating current can be simply determined by subtracting ${i'}_{L,p}$ from the load current i_L as

$$i_C^* = i_L - i'_{L,p} = i_L - \frac{\bar{p}}{v_{g\alpha}^2 + v_{g\beta}^2} v_{g\alpha} \tag{6}$$

where, the term $\bar{p}$ is typically determined by passing the instantaneous power p (i.e., $p = v_{g\alpha} i_{L\alpha} + v_{g\beta} i_{L\beta}$) through a LPF.

To provide a self supporting dc-bus property for APF, a term p_{dc} is also added to (6) as follows

$$i_C^* = i_L - \frac{(\bar{p} + p_{dc})}{v_{g\alpha}^2 + v_{g\beta}^2} v_{g\alpha}. \tag{7}$$

This term is typically generated by passing the difference between the reference value of the dc-bus voltage and its actual value through a proportional-integral (PI) controller.

The major drawback regarding the extraction of reference compensating current using (7) is that, the extraction accuracy highly depends on the grid voltage quality. In other words,

presence of distortion in the grid voltage results in errors in the reference current generation.

III. Suggested RCG Technique

Fig. 2(a) illustrates the basic scheme of the suggested RCG technique, in which the SOGI structures are employed to generate the filtered in-phase and quadrature-phase versions of the grid voltage and load current, i.e., $v'_{g\alpha}$, $v'_{g\beta}$, $i'_{L\alpha}$, and $i'_{L\beta}$, respectively. The scheme of a SOGI is illustrated in Fig. 2(b), where k is the damping factor [23]. In order to obtain a balanced set of in-quadrature outputs with correct amplitudes, the center frequency of the SOGI structure must be equal to the input signal frequency. To achieve this goal, the center frequency is adjusted by an estimation of the grid voltage frequency. The estimated frequency is obtained by using a synchronous reference frame PLL (SRF-PLL). SRF-PLLs have a long history of use in three-phase systems, however in single-phase applications, their implementation is more complicated, because of the lack of multiple independent input signals [24], [25]. To overcome this problem, the generation of a secondary orthogonal phase from the original single-phase grid voltage is necessary. In the suggested approach, as shown, the same in-phase and quadrature-phase versions of the grid voltage (i.e., $v'_{g\alpha}$, and $v'_{g\beta}$) that are used to extract the reference compensating current, are employed in the SRF-PLL. Thus, the need for generating a secondary orthogonal phase for the SRF-PLL is eliminated. At first glance, one may argue that, the precise extraction of the reference compensating current requires considering a high level of filtering (small value of the damping factor k) for SOGI structures, which results in a relatively long settling time for $v'_{g\alpha\beta}$, and $i'_{L\alpha\beta}$. Therefore, considering $v'_{g\alpha\beta}$ as the input signals of the SRF-PLL will result in a very poor dynamic response in estimation of the grid voltage frequency, and may degrade the stability of the PLL. This deduction is true when a PI compensator is used as the loop filter in the SRF-PLL. While, in the suggested structure, a PI-lead controller is employed as the loop filter. Using a detailed mathematical analysis, it will be shown that, how adding a lead compensator to the conventional PI controller significantly improves the dynamic response and the stability margin of the SRF-PLL.

IV. Design Guidelines

A. SOGI Structures

From Fig. 2(b), the characteristic transfer functions of the SOGI block can be obtained as

$$D(s) = \frac{v'_{g\alpha}}{v_g} = \frac{i'_{L\alpha}}{i_L} = \frac{k\hat{\omega}s}{s^2 + k\hat{\omega}s + \hat{\omega}^2} \tag{8a}$$

$$Q(s) = \frac{v'_{g\beta}}{v_g} = \frac{i'_{L\beta}}{i_L} = \frac{k\hat{\omega}^2}{s^2 + k\hat{\omega}s + \hat{\omega}^2}. \tag{8b}$$

Figs. 3(a) and (b) illustrate the Bode plots of the transfer functions (8a) and (8b), respectively, for three different values of damping factor k. As it can be observed, a lower k leads

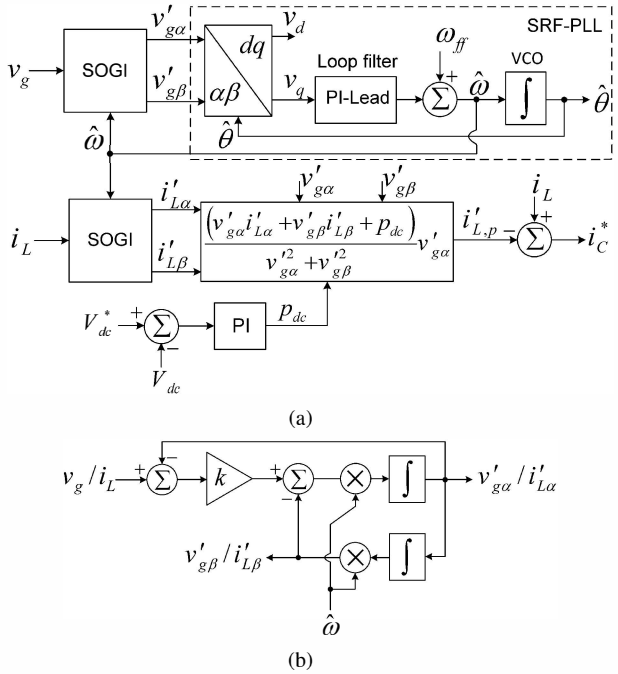

Fig. 2. Suggested RCG technique: (a) basic scheme, and (b) SOGI block.

to a narrower bandwidth, and hence better filtering capability. However, a very low value of k degrades the dynamic performance of the SOGI, resulting in a significant delay in extraction of the reference compensating current. It is well known that, during the load transients, the delay in extraction of the reference current increases the duration for which APF must sink/source the fundamental current, hence increases the required APF rating [7], [26]. Therefore, it is necessary to find a satisfactory compromise between the speed of response and the harmonic rejection.

It can be easily shown that, under the frequency locked condition (i.e., $\omega = \hat{\omega}$), the outputs of the SOGI for a given input voltage $v_g = V cos(\omega t + \phi)$, and for $k < 2$ are

$$v'_{g\alpha}(t) = V\cos(\omega t+\phi)+A_\alpha\cos(\omega\sqrt{1-(k/2)^2}t+\phi_\alpha)e^{-\frac{k\hat{\omega}}{2}t} \tag{9}$$

$$v'_{g\beta}(t) = V\sin(\omega t+\phi)+A_\beta\sin(\omega\sqrt{1-(k/2)^2}t+\phi_\beta)e^{-\frac{k\hat{\omega}}{2}t} \tag{10}$$

where A_α, A_β, ϕ_α, and ϕ_β are functions of V, ϕ, and k. The similar results can be obtained for the load current i_L.

From (9) and (10), it is observed that, the transient terms decay to zero with a time constant of $\tau = 2/k\hat{\omega}$. Thus, by considering a same damping factor k for both SOGI structures in Fig. 2, the settling time for the extraction of the reference current can be approximated as

$$t_s = 4\tau = \frac{8}{k\hat{\omega}}. \tag{11}$$

Based on (11), the damping factor k can be simply determined by deciding an appropriate value for the settling time

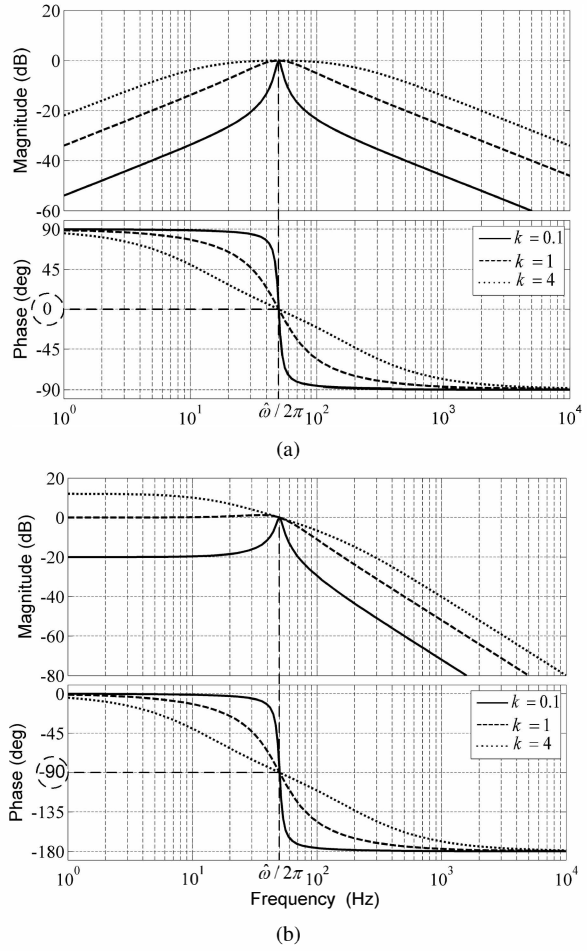

Fig. 3. Bode plots of the characteristic transfer functions of the SOGI block for different values of k: a) $G_\alpha = v_\alpha/v_i$, and b) $G_\beta = v_\beta/v_i$.

t_s. In this paper, t_s is selected to be equal to two cycles of the fundamental frequency, yielding $k = 0.637$.

From the harmonic rejection point of view, the selected value for the damping factor is adequate for low distorted load currents. However, in cases, where the load current have a high harmonic content it may not be adequate. This problem can be simply alleviated by adding extra SOGI blocks in parallel with the single SOGI structure of the load current, as shown in Fig. 4 [23]. Each SOGI block is tuned to resonate at a desired harmonic frequency, and is responsible for attenuating a specific harmonic component in the load current, improving the accuracy of the extraction of the reference compensating current. Hereby, the bandwidth of the fundamental frequency SOGI can be even more increased to achieve faster dynamic performance.

The performance of the multi-SOGI structure shown in Fig. 4 can be better visualized through the Bode diagrams plotted in Fig. 5. The solid line in Fig. 5 indicates the Bode plot of the transfer function $i'_{L\alpha}/i_L$ for a multi-SOGI structure including four modules tuned at the fundamental, third, fifth, and seventh harmonic frequencies, and the dashed line indicates the Bode plot for a single SOGI structure tuned at the

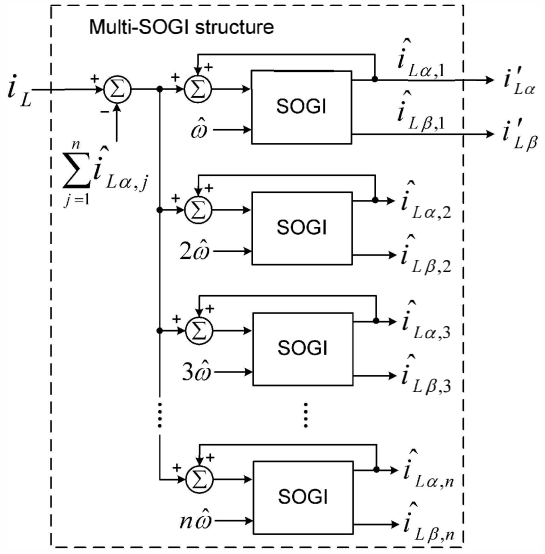

Fig. 4. Multi-SOGI structure.

fundamental frequency. As it can be observed, the added SOGI blocks results in notches in the gain plot at their resonance frequencies. As a consequence, in the case of a highly distorted load current, the extraction error is significantly reduced. It is worth to mention that, the added SOGI blocks do not affect the dynamics of the fundamental component SOGI block, since they only respond to the frequencies around their resonant frequencies, unless very high damping factors are selected for these blocks.

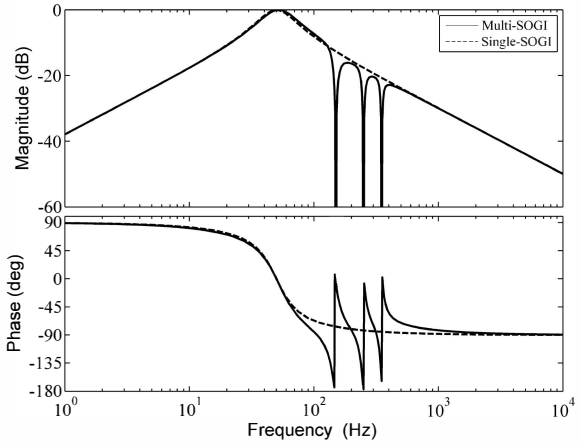

Fig. 5. Bode plots of the Multi-SOGI and single-SOGI structures.

The number of SOGI blocks that need to be added depends on the distortion level in the load current. However, since the computational load is a major limiting factor, a trade-off has to be found between accuracy and computational effort. In this paper, adding two SOGI blocks tuned at the third and fifth harmonic frequencies is suggested, since, typically, they are the most dominant current harmonics produced by single-phase nonlinear loads.

It is worth noting that, under highly distorted grid con-

ditions, as what proposed for the load current, the quality of in-quadrature outputs of the grid voltage SOGI block can be readily enhanced by employing extra harmonic component SOGI blocks.

B. Loop Filter Parameters Design

In this section, a systematic design procedure to fine tune the loop filter parameters is suggested. To simplify the design procedure and the stability analysis, the small-signal model of the SRF-PLL is derived first. Then, the pole-zero cancellation technique and the extended symmetrical optimum theory are employed to design the control parameters.

In order to derive the small-signal model, a quasi-locked state (i.e., $\omega = \hat{\omega}$, and $\phi \approx \hat{\phi}$) is assumed, where $\hat{\omega}$ and $\hat{\phi}$ are the estimated frequency and phase-angle by the PLL, respectively.

1) Small-signal modeling: Let us consider the Park's ($\alpha\beta \rightarrow dq$) transformation as

$$T = \begin{bmatrix} \cos\hat{\theta} & \sin\hat{\theta} \\ -\sin\hat{\theta} & \cos\hat{\theta} \end{bmatrix},\ \hat{\theta} = \hat{\omega}t + \hat{\phi} \tag{12}$$

where, $\hat{\theta}$ is the estimated angle. Applying (12) to ${v'}_{g\alpha}$ and ${v'}_{g\beta}$, gives the loop filter input signal (i.e., v_q) as

$$v_q(t) = -\sin\hat{\theta}{v'}_{g\alpha}(t) + \cos\hat{\theta}{v'}_{g\beta}(t). \tag{13}$$

Substituting (9) and (10) into (13), and performing some mathematical manipulations, yields (14). From (14), it is observed that, the fluctuating terms decay to zero with a time constant of $\tau = 2/k\hat{\omega}$, therefore, v_q can be approximated in the Laplace domain by

$$v_q(s) = \frac{V}{1+\tau s}\phi_e(s) \tag{15}$$

where, $\phi_e = \phi - \hat{\phi}$.

To minimize the phase error ϕ_e, v_q is passed through the loop filter, here a PI-lead controller with the following transfer function

$$LF(s) = \underbrace{\frac{k_p s + k_i}{s}}_{\text{PI}}\underbrace{\frac{1+\tau_1 s}{1+\tau_2 s}}_{\text{Lead}} \tag{16}$$

where k_p and k_i are the proportional and integral gains of the PI controller, respectively, and τ_1 and τ_2 ($\tau_1 > \tau_2$) are the parameters of the lead compensator.

Based on the above information and considering the VCO as an integrator, the small-signal model of the PLL can be obtained as shown in Fig. 6.

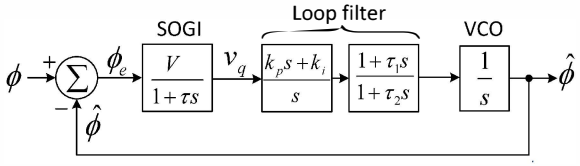

Fig. 6. Small-signal model of the PLL.

2) Pole-zero cancellation (PZC): The relatively large time constant (τ) of the SOGI structure, which is necessary to provide high harmonic rejection in extraction of the reference current, will significantly degrade the dynamic performance and stability margin of the PLL, if it is not compensated properly. That is the reason why a PI-lead controller (instead of a simple PI controller) is suggested as the loop filter in this paper.

The lead compensator introduces an additional pole/zero pair to the system. Thereby, the slow dynamics of the undesirable pole (i.e., $s = -1/\tau$) can be simply canceled, if the zero of the lead compensator (i.e., $s = -1/\tau_1$) is located at the pole position, i.e.,

$$\tau_1 = \tau = 2/k\hat{\omega}. \tag{17}$$

It is worth to mention that, due to the variation of the grid frequency, and hence the estimated frequency, the undesirable pole has a varying nature. Therefore, for a fixed value of τ_1, the exact PZC is not viable. However, since the grid-frequency is typically allowed to change in a narrow band (e.g., $47\,Hz < \omega < 52\,Hz$, as defined in [27]), selecting $\tau_1 = 2/k\omega_{ff}$, where ω_{ff} is the nominal frequency, effectively cancels the influence of the undesirable pole.

3) Symmetrical optimum theory: The symmetrical optimum theory is a standard procedure for designing type-2 control systems with an open-loop transfer function as

$$G_{ol}(s) = K\frac{(T_1 s + 1)}{s^2(T_2 s + 1)}. \tag{18}$$

The main idea of this approach is that to achieve the maximum possible phase margin, the crossover frequency should be at the geometric mean of corner frequencies [28], [29]. Application of this method to the PLL-based frequency synthesizers can be found in [30].

If a perfect PZC is assumed, then the open loop transfer function becomes

$$G_{ol}(s) = V\frac{k_p s + k_i}{s^2(1+\tau_2 s)}. \tag{19}$$

Considering $k_p/k_i = \tau_z$, and $\tau_2 = \tau_p$, (19) can be rewritten as

$$v_q(t) = \underbrace{V\sin(\phi - \hat{\phi})}_{\approx V(\phi-\hat{\phi})} + \left[A_\beta \sin(\omega\sqrt{1-(k/2)^2}\,t + \phi_\beta)\cos(\omega t + \hat{\phi}) - A_\alpha \cos(\omega\sqrt{1-(k/2)^2}\,t + \phi_\alpha)\sin(\omega t + \hat{\phi})\right] e^{-\frac{k\omega}{2}t} \tag{14}$$

$$G_{ol}(s) = Vk_i \frac{1+\tau_z s}{s^2(1+\tau_p s)}. \tag{20}$$

From (20), the crossover frequency (open-loop unity gain frequency , i.e., $|G_{ol}(j\omega_c)| = 1$) can be obtained as

$$\omega_c = Vk_p \frac{\cos\varphi_p}{\sin\varphi_z} \tag{21}$$

where

$$\varphi_p = \tan^{-1}(\tau_p \omega_c) \tag{22a}$$

$$\varphi_z = \tan^{-1}(\tau_z \omega_c). \tag{22b}$$

The phase margin (i.e., the difference between 180 degrees and the phase angle of the open loop transfer function at the cross-over frequency) is

$$PM = 180 + \measuredangle G_{ol}(j\omega_c) = \varphi_z - \varphi_p. \tag{23}$$

To ensure the stability, the phase margin should be maximized. This goal can be simply realized by differentiating (23) with respect to ω_c and equating the result to zero, which leads to

$$\omega_c = \frac{1}{\sqrt{\tau_z \tau_p}}. \tag{24}$$

As it can be concluded from (24), for given values of τ_z and τ_p, the PLL phase margin is maximized if the crossover frequency is equal to the geometric mean of the corner frequencies $1/\tau_z$ and $1/\tau_p$.

Based on (22) and (24), it is easy to show that

$$\sin\varphi_z = \cos\varphi_p \tag{25a}$$

$$\varphi_z + \varphi_p = 90^\circ. \tag{25b}$$

Substituting (25a) into (21), gives

$$\omega_c = Vk_p. \tag{26}$$

Substituting (25b) into (23), and performing some mathematical manipulations, gives

$$\tau_z = \frac{1}{\omega_c}\tan(45^\circ + PM/2) \tag{27a}$$

$$\tau_p = \frac{1}{\omega_c}\tan(45^\circ - PM/2). \tag{27b}$$

From (26) and (27), the loop filter parameters k_p, k_i, and τ_2 can be expressed based on w_c and PM, as

$$\begin{cases} k_p = \omega_c/V \\ k_i = k_p/\tau_z = \dfrac{\omega_c^2}{V\tan(45^\circ + PM/2)} \\ \tau_2 = \tau_P = \dfrac{1}{\omega_c}\tan(45^\circ - PM/2). \end{cases} \tag{28}$$

An interesting observation from (28) is that, in an optimum manner, the number of degrees of freedom is reduced by one. In other words, the loop filter parameters (i.e. k_p, k_i, and τ_2) can be determined by selecting appropriate values for the crossover frequency ω_c and the phase margin PM.

The recommended range for the phase margin is between 30° and 60° [31]. In this paper, a PM in the middle of this range, i.e., $PM = 45^\circ$, is selected. For the crossover frequency ω_c, the situation is a bit more complex. A high value of ω_c improves the dynamic performance of the PLL, but at the expense of noise/disturbance rejection capability of the PLL. Consequently, selection of the crossover frequency is a tradeoff between the dynamic response and the noise/disturbance rejection capability. In this paper, based on extensive simulation results, w_c is selected to be $2\pi 20\,\mathrm{rad/s}$.

By substituting the selected values of the phase margin and the crossover frequency (i.e., $PM = 45^\circ$ and $\omega_c = 2\pi 20\,\mathrm{rad/s}$) into (28), the loop filter parameters are determined as follows

$$\begin{cases} k_p = 125.66 \\ k_i = 6541 \\ \tau_2 = 3.296e-3\,s. \end{cases} \tag{29}$$

Notice that, to determine the parameters, the input voltage amplitude V was assumed to be unity. This assumption can be simply realized by dividing the loop filter input signal (i.e., v_q) by an estimation of the input voltage amplitude prior to being fed into the loop filter.

Fig. 7 illustrates the Bode plot of the open-loop transfer function (19) for the designed parameters. As expected, the crossover frequency corresponds to the peak of the phase plot, optimizing the PLL phase margin. The system gain margin (GM), as shown, is infinite.

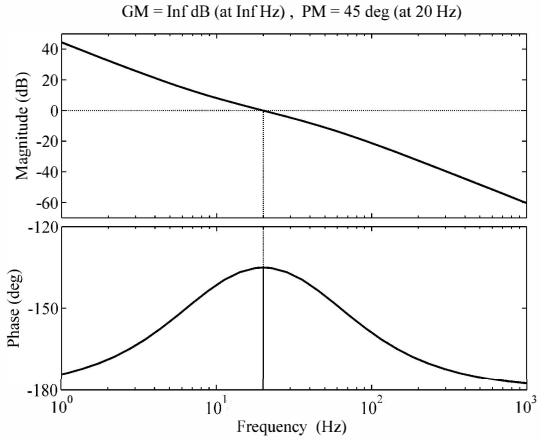

Fig. 7. Bode plot of the open-loop transfer function.

V. Simulation Results

In this section, the performance of the suggested RCG technique is evaluated on a simple distribution system loaded with diode bridge rectifiers (DBRs), as shown in Fig. 8. The load current and grid voltage are sensed at the point of connection, and fed to the suggested RCG technique to extract the reference compensating current. The simulation studies are

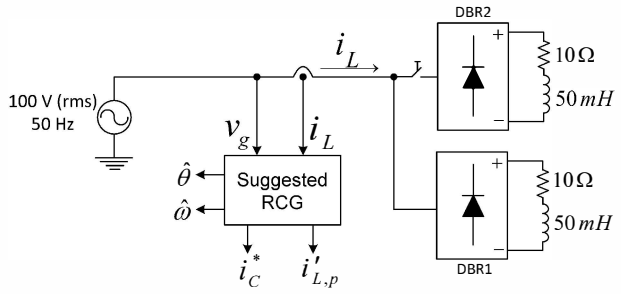

Fig. 8. Simple distribution system used to confirm the performance of the suggested RCG.

carried out in Matlab/Simulink. The sampling frequency is fixed to 10 kHz, and the nominal frequency is set to 50 Hz.

In the suggested RCG, a dual-SOGI structure (tuned at the fundamental, and third harmonic frequencies) for the grid voltage, and a multi-SOGI structure (including three modules tuned at the fundamental, third and fifth harmonic frequencies) for the load current are employed.

A. Load Change

In the first test, the supply voltage consists of a 1-p.u. fundamental component, a 0.05-p.u. third harmonic, a 0.05-p.u. fifth harmonic, and a 0.1-p.u. seventh harmonic. Initially, DBR1 is in service, and the system is in the steady-state condition. At t=20 ms, DBR2 is switched on. Figs. 9(a), (b), and (c) illustrate the grid voltage, the load current, and the extracted reference current (i_C^*), respectively. The grid voltage total harmonic distortion (THD) is 12.1%, and the load current THD is 43.96%. Figs. 9(d) and (e) illustrate the extracted fundamental active current component ($i'_{L,P}$) and the estimated frequency of grid voltage, respectively. Notice that, $i'_{L,P}$ is in-phase with the fundamental component of the supply voltage. As expected, the settling time for extracting the reference compensating current is around two cycles of the fundamental frequency.

B. Grid Frequency Step Change

In this test, DBR1 is in service, and the supply voltage harmonic components are the same as before. Suddenly, at t=20 ms, the supply voltage undergoes a frequency step change of +5 Hz. Fig. 10 illustrates the simulation results under this scenario. As it can be seen, the steady-state is achieved fast. Therefore, the robustness of the suggested RCG against grid frequency variations is proved.

VI. Conclusion

A simple and effective implementation of the single-phase pq theory to extract the reference compensating current for the single-phase SAPFs has been proposed in this paper. The SOGIs were employed as the basic building blocks of the suggested approach. To fine tune the control parameters, a systematic approach based on the pole-zero cancellation, and the extended symmetrical optimum theory has been proposed. Effectiveness of the suggested approach has been confirmed through simulation results.

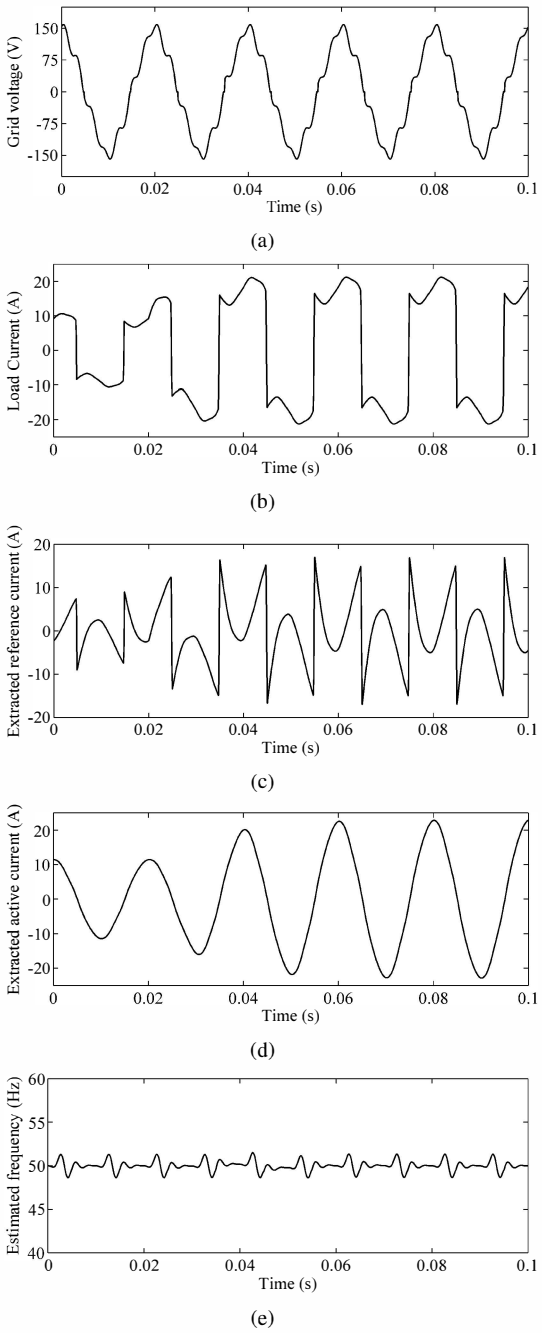

Fig. 9. Simulation results in response to a load change.

References

[1] C. Lascu, L. Asiminoaei, I. Boldea, and F. Blaabjerg, "High performance current controller for selective harmonic compensation in active power filters," *IEEE Trans. Power Electron.*, vol. 22, no. 5, pp. 1826-1835, Sep. 2007.

[2] D. Yazdani, A. Bakhshai, G. Joos, and M. Mojiri, "A real-time three-phase selective-harmonic-extraction approach for grid-connected converters," *IEEE Trans. Ind. Electron.*, vol. 56, no. 10, pp. 4097-4106, Oct. 2009.

[3] F. D. Freijedo, J. Doval-Gandoy, O. Lopez, P. Fernandez-Comesana, and C. Martinez-Penalver, "A signal-processing adaptive algorithm for selective current harmonic cancellation in active power filters," *IEEE Trans. Ind. Electron.*, vol. 56, no. 8, pp. 2829-2840, Aug. 2009.

[4] A. Varschavsky, J. Dixon, M. Rotella, and L. Moran, "Cascaded nine-level

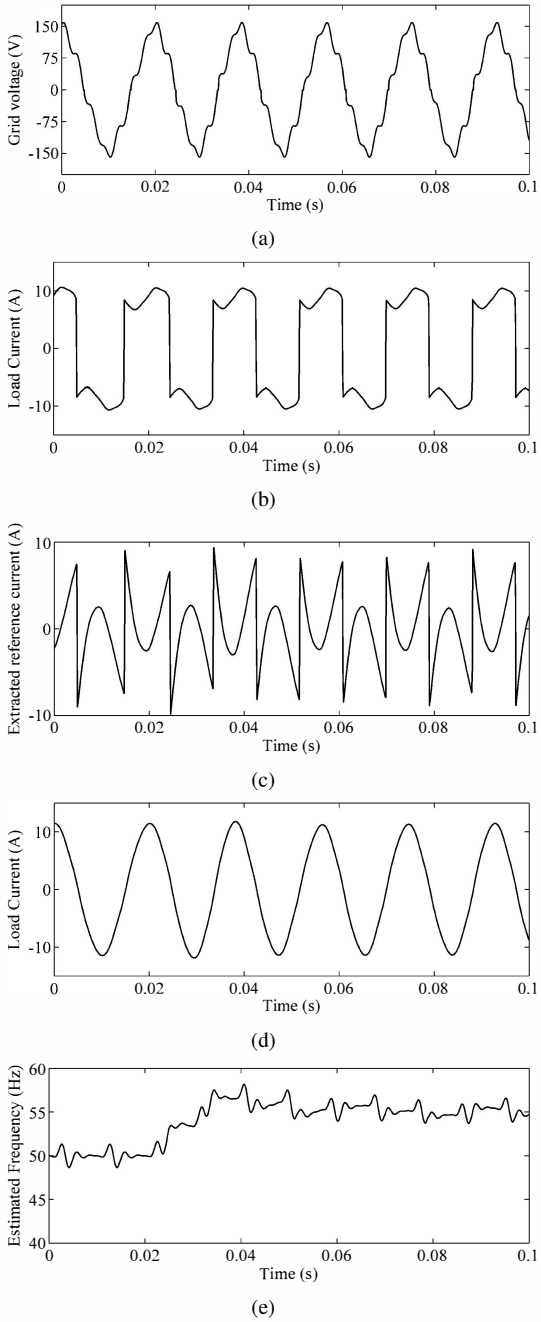

Fig. 10. Simulation results in response to a frequency step change.

inverter for hybrid-series active power filter, using industrial controller," *IEEE Trans. Ind. Electron.*, vol. 57, no. 8, pp. 2761-2767, Aug. 2010.

[5] J. Matas, L. G. de Vicuna, J. Miret, J. M. Guerrero, and M. Castilla, "Feedback linearization of a single-phase active power filter via sliding mode control," *IEEE Trans. Power Electron.*, vol. 23, no. 1, pp. 116-125, Jan. 2008.

[6] J. M. Maza-Ortega, J. A. Rosendo-Macias, A. Gomez-Exposito, S. Ceballos-Mannozzi, and M. Barragan-Villarejo, "Reference current computation for active power filters by running DFT techniques," *IEEE Trans. Power Del.*, vol. 25, no. 3, pp. 446-456, Jul. 2010.

[7] R. Chudamani, K. Vasudevan, and C. S. Ramalingam, "Non-linear least-squares-based harmonic estimation algorithm for a shunt active power filter," *IET Power Electron.*, vol. 2, no. 2, pp. 134-146, Mar. 2009.

[8] B. P. McGrath, D. G. Holmes, and J. J. H. Galloway, "Power converter line synchronization using a discrete Fourier transform (DFT) based on variable sampling rate," *IEEE Trans. Power Electron.*, vol. 20, no. 4, pp. 877-884, Jul. 2005.

[9] L. Asiminoaei, F. Blaabjerg, and S. Hansen, "Detection is key-Harmonic detection methods for active power filter applications," *IEEE Ind. Appl. Mag.*, vol. 13, no. 4, pp. 22-33, Jul./Aug. 2007.

[10] E. Jacobsen, and R. Lyons, "The sliding DFT," *IEEE Signal Process. Mag.*, vol. 20, no. 2, pp. 74-80, Mar. 2003.

[11] H. Li, F. Zhuo, Z. Wang, W. Lei, and L. Wu, "A novel time-domain current-detection algorithm for shunt active power filters," *IEEE Trans. Power Syst.*, vol. 20, no. 2, pp. 644-651, May 2005.

[12] H. Wang, Q. Li, and M. Wu, "Investigation on a new algorithm for instantaneous reactive and harmonic currents detection applied to intensive nonlinear loads," *IEEE Trans. Power Del.*, vol. 22, no. 4, pp. 2312-2318, Oct. 2007.

[13] H. Akagi, Y. Kanazawa, and A. Nabae, "Instantaneous reactive power compensators comprising switching devices without energy storage components," *IEEE Trans. Ind. Appl.*, vol. IA-20, no. 3, pp. 625-630, May/Jun. 1984.

[14] H. Akagi, Y. Kanazawa, and A. Nabae, "Generalized theory of the instantaneous reactive power in three-phase circuits," *in Proc. IPEC*, 1983, pp. 1375-1386.

[15] M. Aredes, H. Akagi, E. H. Watanabe, S. E. Vergara, and L. F. Encarnacao, "Comparisons between the p-q and p-q-r theories in three-phase four wire systems," *IEEE Trans. Power Electron.*, vol. 24, no. 4, pp. 924-933, Apr. 2009.

[16] J. C. Montano, "Reviewing concepts of instantaneous and average compensations in polyphase systems," *IEEE Trans. Ind. Electron.*, vol. 58, no. 1, pp. 213-220, Jan. 2011.

[17] J. Liu, J. Yang, and Z. Wang "A new approach for single-phase harmonic current detecting and its application in a hybrid active power filter," *in Proc. Annu. Conf. IEEE Indust. Electron. Soc. (IECON99)*, 1999, vol. 2, pp. 849-854.

[18] M. T. Haque, "Single phase PQ theory for active filters," *in Proc IEEE TENCON'02, 2002*, pp. 1941-1944.

[19] H. Akagi, E. H. Watanabe, and M. Aredes, *Instantaneous power theory and applications to power conditioning*. Piscataway, NJ/New York: IEEE Press/Wiley-Interscience, 2007.

[20] M. Saitou, and T. Shimizu, "Generalized theory of instantaneous active and reactive powers in single-phase circuits based on Hilbert transform," *in Proc. 33rd Annu. IEEE PESC*, Jun. 2002, pp. 1419-1424.

[21] V. Khadkikar, M. Singh, A. Chandra, and B. Singh, "Implementation of single-phase synchronous dq reference frame controller for shunt active filter under distorted voltage condition," *in Proc. IEEE PEDES Conf.*, Dec. 2006, pp. 1-6.

[22] V. Khadkikar, A. Chandra, and B. N. Singh, "Generalised single-phase p-q theory for active power filtering: Simulation and DSP-based experimental investigation," *IET Power Electron.*, vol. 2, no. 1, pp. 67-78, Jan. 2009.

[23] P. Rodriguez, A. Luna, I. Candela, R. Mujal, R. Teodorescu, and F. Blaabjerg, "Multiresonant frequency-locked loop for grid synchronization of power converters under distorted grid conditions," *IEEE Trans. Ind. Electron.*, vol. 58, no. 1, pp. 127-138, Jan. 2011.

[24] S. Golestan, M. Monfared, F. D. Freijedo, J. M. Guerrero, "Design and tuning of a modified power-based PLL for single-phase gridconnected power conditioning systems," *IEEE Trans. Power Electron.*, vol. 27, no. 8, pp. 3639-3650, Aug. 2012.

[25] S. Golestan, M. Monfared, F. D. Freijedo, and J. M. Guerrero, "Dynamics assessment of advanced single-phase PLL structures," *IEEE Trans. Ind. Electron.* vol. PP, no. 99, pp.1-11, Apr. 2012.

[26] T. C. Green, and J. H. Marks, "Ratings of active power filters," *IEE Proc.-Electr. Power Appl.*, vol. 150, no. 5, Sep. 2003.

[27] *Voltage Characteristics of Electricity Supplied by Public Distribution Systems*, European Standard EN 50160, 2008.

[28] S. Preitl and R.-E. Precup, "An extension of tuning relations after symmetrical optimum method for PI and PID controller," Automatica, vol. 35, no. 10, pp. 17311736, Oct. 1999.

[29] R. Teodorescu, M. Liserre, and P. Rodriguez, *Grid Converters for Photovoltaic and Wind Power Systems*. New York: IEEE-Wiley, 2011.

[30] K. Shu and E. Sanchez-Sinencio, *CMOS PLL Synthesizers-Analysis and Design*. New York: Springer, 2005.

[31] R. C. Dorf and R. H. Bishop, *Modern Control Systems*, 9th ed. Englewood Cliffs, NJ: Prentice-Hall, 2000.